ACS APPLIED MATERIALS & INTERFACES

Article

Polymeric 3D printed functional microcantilevers for biosensing applications

Stefano Stassi, Erika Fantino, Roberta Calmo, Annalisa Chiappone, Matteo Gillono, Davide Scaiola, Candido Fabrizio Pirri, Carlo Ricciardi, Alessandro Chiado', and Ignazio Roppolo

ACS Appl. Mater. Interfaces, **Just Accepted Manuscript** • Publication Date (Web): 22 May 2017

Just Accepted

ACS Publications

ACS Applied Materials & Interfaces is published by the American Chemical Society.
1155 Sixteenth Street N.W., Washington, DC 20036

Polymeric 3D Printed Functional Microcantilevers for Biosensing Applications

Stefano Stassi[a,‡], *Erika Fantino*[a,‡], *Roberta Calmo*[a,‡], *Annalisa Chiappone*[b], *Matteo Gillono*[a,b], *Davide Scaiola*[a], *Candido Fabrizio Pirri*[a,b], *Carlo Ricciardi*[a], *Alessandro Chiadò*[a],*, *Ignazio Roppolo*[b],*

[a] Department of Applied Science and Technology, Politecnico di Torino, Corso Duca degli Abruzzi 24, 10129 Torino, Italy

[b] Center for Sustainable Future Technologies, Istituto Italiano di Tecnologia, Corso Trento 21, Torino, 10129 Italy

KEYWORDS: 3D printing, Microcantilever, Biosensors, DLP, Mechanical Resonators

ABSTRACT

The present work shows for the first time the production of mass sensitive polymeric biosensors by 3D printing technology with intrinsic functionalities. We demonstrate the feasibility of mass sensitive biosensors in the form of microcantilever in a one-step printing process, using acrylic acid as functional co-monomer for introducing a controlled amount of functional groups that can

covalently immobilize the biomolecules onto the polymer. The effectiveness of the application of 3D printed microcantilevers as biosensors is then demonstrated with their implementation in a standard immunoassay protocol. This work shows how 3D microfabrication techniques, material characterization and biosensor development could come together to obtain an engineered polymeric microcantilever with intrinsic functionalities. The possibility of tuning the composition of the starting photocurable resin with the addition of functional agents, and consequently control the functionalities of the 3D printed devices, paves the way to a new class of mass sensing MEMS devices with intrinsic properties.

Introduction

Resonant mechanical structures have been widely used in the last decades as highly sensitive mass sensing devices.[1] Thanks to their high resolution and simplicity of measurement, microresonators were successfully implemented for biological, chemical and agroindustrial applications.[2-4] Moreover, the need of pushing forward the limit of detection to analyze small particles like viruses, DNA or nanoparticles, increased the development of mechanical resonators shrinking geometry and mass of the devices, with a noteworthy enhancement of the sensitivity. Mass resolution in the zeptogram range was obtained decreasing thickness of the silicon resonator in the nanometer scale[5] and even yoctogram sensitivity was reached using bottom-up integrated nanomechanical resonators such as carbon nanotubes.[6] However, these micro and nanoresonator devices mostly require expensive and time consuming micro and nanofabrication techniques, which limit their implementation as standard chemical and biological sensors. In addition, cantilever sensors are usually fabricated in silicon or silicon based materials (such as silicon dioxide or silicon nitrate) and thus present an inert surface, which interacts with

molecules mostly by physisorption phenomena, without any selectivity.[7, 8] An additional functionalization step is then needed to reach the sensitivity and selectivity required to detect biological or chemical analytes.[9] This process further increases the sensor preparation time and often requires the implementation of hazardous and/or persistent chemicals in an anhydrous environment.

In order to overcome these functionalization issues, different kinds of polymers have been used to prepare ultrasensitive biosensors[10] and to develop polymeric cantilevers. In fact, the use of polymeric materials allows easier integration of the biorecognition elements, both by incorporation[11] or chemical reaction,[12] taking advantages of the functional groups already present. In particular, cantilever based on SU8 (a photocurable epoxy resin)[13, 14], PDMS[15, 16] and PEGDA[17, 18] were developed. However, the fabrication of these devices is still very complex and time consuming since it is based on standard lithographic techniques.

The fabrication of 3D microstructures is typically complex and requires time-consuming multistep processes. In this context, 3D printing represents an intriguing alternative in order to overcome both technological and functionalization issues, allowing the fabrication of reliable and ready-to-use mechanical resonator sensors in a single fabrication step. In fact, 3D printing allows the direct fabrication of objects starting from CAD files, which represents a time-saving and cost-effective approach both in sensor prototyping and in fabrication. The digital image of the object is sliced by a dedicated software and the component is built in the printer layer-by-layer.[19] Among the different 3D printing methods for polymeric materials, the technologies based on photopolymerization (such as steoreolithography (SLA), digital light processing (DLP), and two photon polymerization (2PP)) result particularly helpful for the fabrication of functional materials.[20] In fact, those techniques involve the use of liquid photocurable resins which could be

easily modified playing on the ingredients in the starting formulations, tailoring the final properties of the printed objects.[21, 22] For instance, it is possible to introduce novel functionalities to the polymer networks adding in the printable formulation fillers[23-25] or precursors of metallic/ceramic phase[26-28] or properly selecting photocurable monomers with chemically active groups. [29-32]

To the best of our knowledge, few examples of cantilever produced by 3D printing technologies are reported in the literature: Watanabe et al. produced light responsive hydrogels with a cantilever shape by 2PP,[33] whereas Gomez et al. used a 2PP approach for the production of microcantilever (MCs) made of Molecular Imprinted Polymers.[34] More recently, Credi et al. reported about nanocomposites containing magnetic nanoparticles printed by SLA with a cantilever shape in the millimeter range.[35] Therefore, 3D printing technology can be exploited to fabricate in a single step polymeric microcantilevers; however, in most of the cases the cantilever shape was chosen just for investigating mechanical/deformation properties and not as functional mechanical structure for sensors. Thus, it is possible to envisage the production of chemical and biological sensors with intrinsic functionalities by properly tailoring the formulation composition.

The present work shows for the first time the production of mass sensitive biosensors by 3D printing technology with intrinsic functionalities. The printed device, composed by an array of MCs, was prepared from an acrylic-based formulation with the addition of acrylic acid acting as functionalization agent. Acrylic acid (AA) was chosen as a co-monomer to control the number of carboxyl group available on the microcantilevers. This approach is alternative to the classical functionalization step, normally based on an anhydrous 3-aminopropyltriethoxysilane (APTES) silanization, needed toward biosensing to prepare the silicon surface of standard microcantilevers

for the immobilization of biomolecules. At first, a chemical and functional characterization of the material has been performed. Afterwards, an immunoassay was used as a proof of concept of the application of 3D printed microcantilever as biosensors, demonstrating the possibility to fabricate devices with intrinsic properties by tuning the composition of the printable formulation.

Experimental Section

Materials and chemicals: Bisphenol A ethoxylate diacrylate, BEDA (EO/phenol 2, Mn 512) and Acrylic Acid (AA) were purchased from Sigma Aldrich and used as received. Bis-(2,4,6-trimethylbenzoyl) phenylphosphineoxide (Irgacure 819, BASF) was selected as initiating system for his absorbing characteristics in the deep blue to near UV and was added to the formulations. Reactive Orange 16 (RO, Sigma Aldrich) was also added as a dye to limit light penetration during printing. The recombinant protein G (PtG) was purchased from Thermo Scientific (Fischer Scientific, Milan, IT). The horseradish peroxidase conjugated goat anti-mouse IgG (Ab-HRP) was bought from Merk-Millipore (Milan, Italy). During each step water from MilliQ (Merck-Millipore) was used. 3-aminopropyltriethoxysilane (APTES, anhydrous, 99%), succinic anhydride (SA, 99%), toluene (anhydrous, 99.8%), tetrahydrofuran (THF, 99.9%), triethylamine (TEA), 2-(N-morpholino)ethanesulfonic acid (MES, 99.5%), sodium chloride (99.5%), sulphuric acid (98%, w/w), hydrogen peroxide (30%, w/w), 3,3',5,5'-tetramethylbenzidine (TMB), 1-ethyl-3-(3-dimethylaminopropyl)-carbodiimide (EDC, 99%), N-hydroxy-sulfo-succinimide sodium salt (sulfo-NHS, 98%), Dulbecco's Phosphate Buffer Saline (PBS), polyoxyethylene-glycol-sorbitan monolaurato (Tween-20™), and bovine serum albumin (BSA, protease free, 98%) were purchased from Sigma Aldrich (Milan, Italy) and used without further purification.

3D samples and microcantilever array preparation: Mixtures containing BEDA, Acrylic Acid (0, 5, 10, 20 % wt. in the monomer formulation), photoinitiator (2 per hundred resins, phr) and

RO were prepared (0.2 phr). A Freeform Pico Plus 39 DLP printer (Asiga) with XY pixel resolutions of 39 microns using a LED light source (405 nm, intensity 22 mW/cm^2) was used as printing equipment (see Figure S1 for the printing scheme). The build area is 50 mm × 30 mm × 150 mm and the layer thickness is adjustable from 10 to 100 μm. For every formulation, flat specimens (30 mm × 30 mm × 0.5 mm) were printed; the layer thickness was fixed to 25 μm, the exposure times used ranged from 0.6 s to 1 s per layer accordingly to the printed formulation. For the microcantilever array structure the layer thickness was fixed to 25 μm with an exposure time of 0.8 s per layer for the selected formulation (10 % AA). A post curing process performed with a medium pressure mercury lamp (5 minutes in a lamp provided by Robot Factory, light intensity 10 mW/cm^2) followed the printing process. The digital models of structures were designed and converted to STL file format for 3D printing.

Quantification of the available carboxyl groups: The density of carboxyl groups available for biomolecules covalent binding was estimated by Toluidine Blue O (TBO) colorimetric titration. This cationic dye binds electrostatically to deprotonated carboxyl acid functionalities in an equimolar ratio at high pH values (pH ≈10), and it can be measured by visible absorption at a wavelength of approximately 600-650 nm.[36, 37] In order to promote the interaction, the samples containing different concentration of AA were incubated with 3 mL of 0.5 mM TBO aqueous solution (pH 10) at 37 °C for 5 h. A sample without RO (called BEDA) was also included as a control. To remove the unbound dye, the substrates were rinsed thrice with 3 mL of 0.1 mM NaOH solution. The release of the dye molecules reacted with the –COOH terminations of the AA functionalities was promoted by 1 mL of 50% (v/v) acetic acid solution at pH<2. The optical density (OD) of the recovered solutions was measured at 630 nm (dye maximum absorption) by means of a 2100-C microplate reader (Ivymen Optic System). To determine the density of

available carboxyl groups, a calibration curve made of TBO serially diluted in 50% (v/v) acetic acid at various concentration was also measured and used to estimate the number of TBO molecules, and subsequently of AA functionalities, according to the Lambert–Beer Law.[38] Each condition was analyzed in triplicate and the mean values ± their half-deviation were calculated. In order to obtain a relative quantification of the carboxyl groups available for biomolecule binding, the average value obtained by the BEDA sample was used as a background and subtracted from the other ones.

Functional evaluation of the binding capability by PtG/Ab-HRP colorimetric bioassay: The samples (BEDA + different AA %) were activated by using the protocol by Chiadò *et al.* [39] In details, samples were equilibrated in MES buffer (100 mM MES, 150 mM NaCl, pH 4.7) for 15 minutes, then incubated in a mixture of EDC (4 mM) and sulfo-NHS (10 mM) in MES buffer for 15 minutes. Afterward, the samples were rinsed thrice in PBS supplemented with 0.05% Tween-20™ (PBS-t) to remove the excess of EDC and sulfo-NHS, and incubated overnight at 4 °C with 50 µL of 50 µg/mL of PtG in PBS-t. The same activation protocol was used for the APTES/SA functionalized silicon controls. Negative controls (no PtG) were also included. The day after, the samples were rinsed thrice with PBS-t, incubated in 1% BSA in PBS for 1 h at room temperature and finally with 50 µL of 2 µg/mL of Ab-HRP for 1 h at room temperature. In conclusion, the substrates were washed three times with PBS-t, colorimetrically developed with TMB liquid substrate and stopped with 0.5 M H_2SO_4, at a 1:1 TMB:H_2SO_4 ratio. The OD of the solution was immediately measured at 450 nm and at 630 nm by means of a 2100-C microplate reader (Ivymen Optic System). To quantify the amount of proteins immobilized on the surface, an in-liquid titration curve with serially diluted Ab-HRP in PBS-t was prepared and the related OD was measured. The OD values related to the samples were normalized and transformed in

surface density (molecules/cm^2) by comparison with the in-liquid titration curve, as previously reported.[9] In the tests, three replicates for each experimental condition were used and data reported are the mean values ± their half-deviation. The same protocols were applied to MC arrays, unless that after each incubation the MCs arrays were rinsed thrice with PBS-t, and thrice with Milli-Q™ water, as usually performed with other MC bio-functionalizations.[9]

As comparison, silicon squared samples (5×5 mm^2) were silanized and further derivatized to expose a homogeneous layer of carboxylic groups as previously described elsewhere.[39] In details, the samples were cleaned with a piranha solution (3:1 H_2SO_4:H_2O_2) and silanized with a 1% (v/v) solution of APTES in anhydrous toluene at 70 °C for 10 minutes. Then, APTES/SA samples were obtained by incubation in 50 mM SA and 5% TEA in THF for 2 hours at room temperature.

Materials and Cantilever Characterization: Real-time rheological measurements were performed using an Anton Paar rheometer (Physica MCR 302) in parallel plate mode with a Hamamatsu LC8 lamp with visible bulb and a cutoff filter below 400 nm equipped with 8 mm light guide. The gap between the two rheometer plates was set to 0.1 mm. During the experiments, the sample was kept at a constant temperature (25 °C) and under a constant shear frequency (10 Hz); according to preliminary amplitude sweep tests, all the measurements were performed within the linear viscoelastic (LVE) range at a strain amplitude of 0.2%; the irradiating light was turned on after 2 min in order to stabilize the system prior to initiate the photopolymerization process. Concomitant changes in viscoelastic material moduli during polymerization were measured as a function of exposure time.

ATR spectra were collected on a Tensor 27 FTIR Spectrometer, 16 spectra were collected per each sample with a resolution of 2 cm^{-1} in the range 4000-600 cm^{-1}.

DMTA measurements were performed on 3D printed flat samples (20x10x0.5 mm) with a Triton Technology TTDMA. All the experiments were conducted with a temperature ramp of 3 °C/min, applying a force with frequency of 1 Hz and with 20 μm of displacement.

Contact angle measurements were performed with water (γ = 72.8 mN/m) by means of First Ten Angstroms (Portsmouth, VA, USA) 1000 C instrument, equipped with a video camera and image analyzer, at room temperature with the sessile drop technique. Optical images of the samples were collected with a Leica DM2500 microscope.

Resonance frequency spectra of 3D printed microcantilever were measured with a laser Doppler vibrometer system (MSA-500, Polytec Gmbh). The samples were mounted with an adhesive tape on a piezoelectric disk actuator placed inside a vacuum chamber. During the measurement, a vacuum level around 10^{-7} mbar was reached by means of a turbomolecular and membrane pumps connected in series (MINI-Task System, Varian Inc. Vacuum Technologies). For the bioassay, resonance frequencies of the 3D printed MCs were measured on the as-prepared samples, after the PtG incubation and after the Ab-HRP step. Before each vibration characterization, the MCs were dried in dynamic vacuum conditions.

Results and Discussion

Preliminary studies on printable formulations

The aim of this work was to develop a method for producing cantilevers to be used as microgravimetric sensors by 3D DLP printing technique. Based on previous experience,[40] BEDA was chosen as fundamental oligomer since, when exposed to light in the presence of a suitable photoinitiator, it forms a polymer network that is in the glassy state at room temperature and rigid enough to be tested for the envisaged application. AA was directly added as a co-monomer in the liquid formulation, in order to obtain, in a single fabrication step, functionalized microstructures with a controlled number of carboxyl groups that can be exploited to immobilize the biomolecules used for biosensing.

Prior to the printing step, the influence of the addition of different amounts of AA on the visible light-induced polymerization kinetics was investigated by means of photorheology. The variation of G′ modulus during light irradiation was measured under constant oscillation frequency. **Figure 1A** reports the curves relative to the pure BEDA formulation compared to the ones containing different amounts of AA. The plots show that an increasing amount of AA causes a slight delay on the beginning of the rise of elastic modulus since the addition of a monofunctional reagent leads to the formation of a more loosely cross-linked network with a lower elastic component. The observed delay suggests the need of longer exposure time during printing. In any case, the gel point, that gives an estimate of the time at which the resin begins to gel (represented as the crossover point G'=G'', see supporting info, Fig. S2), always reached in less than 18 seconds for a layer thickness of 100 μm. On the basis of our experience, these times are suitable for DLP-3D printing process.[26, 27]

After the evaluation of the behavior of the formulations under irradiation, the most suitable printing parameters (i.e. layer thickness and exposure time, see Experimental Section) were defined for each formulation. ATR experiments were performed on the printed samples in order

to confirm the copolymerization between the BEDA and AA monomers (see SI for full IR analysis and spectra, Figure S3-S9). The decrease of the peak correspondent to the acrylic double bond stretching (1640 cm^{-1}) demonstrates that the AA effectively enters in the polymeric network, copolymerizing with the BEDA bifunctional monomer.

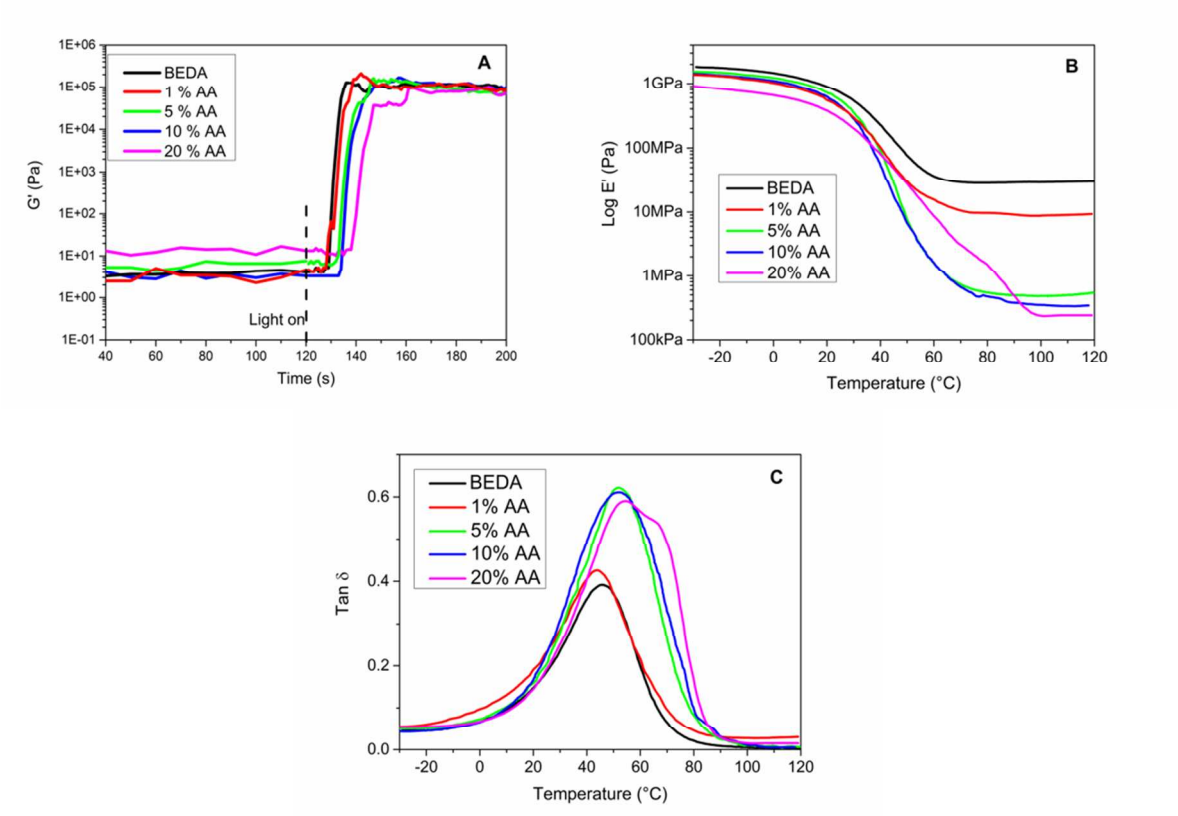

Figure 1. A) Photorheology test: Elastic modulus G' of the curable formulations vs irradiation time. B) Digital model of the printed cantilevers; inset: picture of the 3D cantilever. B) Storage modulus E' of the printed polymers obtained by DMTA tests; C) tan δ of the printed samples obtained by DMTA tests.

The influence of the presence of AA on the thermal/mechanical properties of the printed networks was evaluated by means of DMTA analysis (Figure 1B and Figure 1C). As expected, the introduction of increasing amount of AA in the photocurable formulations induces a decrease of crosslinking density (evidenced in E' value in the rubbery plateau)[41] and an increase of T_g (maximum of tan δ curve) to values closer to 100 °C (T_g of polyAA is around 110 °C).[42] Moreover, tan δ peak shows an important broadening that could be related to a widening in the cross-linking density range. Everything could be explained considering that during photopolymerization the AA copolymerizes with the BEDA monomer, as demonstrated by ATR measurements. Since AA is a monofunctional monomer, its presence leads to the formation of networks with lower cross-linking density with a random distribution of chain length between two cross-linking points. As a result, the DMTA curves show a broader tan δ peak and an evident decrease of E' values in the rubbery plateau with the increase of AA amount in the formulations. Those effects are in good agreement with the literature[43] and confirm that copolymerization occurred during 3D printing of samples, resulting in matrices containing an increased amount of carboxyl moieties.

The influence of hydrophilic AA monomers could be evaluated also by water contact angle measurements. As expected, the hydrophilicity increased along with the AA content (see **Figure 2**). In detail, the value determined for the BEDA sample was of 77.9 ± 0.4 °, while the presence of the dye into the polymer matrix slightly increases the hydrophilicity (64.2 ± 2.2 °). The more hydrophilic sample was the one prepared with 20% of AA, which gave the lowest value (43.4 ± 0.1 °). This value is comparable with those obtained by plasma polymerization of AA on silicon substrates, or by means of the APTES/SA functionalization.[39] A similar result was obtained also

with the sample prepared from 10% of AA (46.6 ± 0.2 °), indicating the saturation of accessible carboxyl groups.

As a result, adding AA in the printable formulations leads to polymeric networks with lower crosslinking density and higher hydrophilicity. However, not all the carboxyl groups coming from the AA monomers will be available for the functionalization step due to intrinsic hindering. For this reason, an evaluation of available carboxyl groups was performed with Toluidine Blue O (TBO), a dye that is positively charged in basic conditions, it interacts electrostatically with negatively charged groups [36, 37] and can be easily detected by visible spectroscopy.[44]

In order to quantitatively estimate the number of available carboxyl groups, a colorimetric titration with TBO has been performed on the different samples (BEDA + different AA %). A sample of pristine BEDA was also included as a control. The average value obtained by the BEDA samples was subtracted from the other ones, in order to obtain a relative quantification of the carboxyl groups available for biomolecules binding.

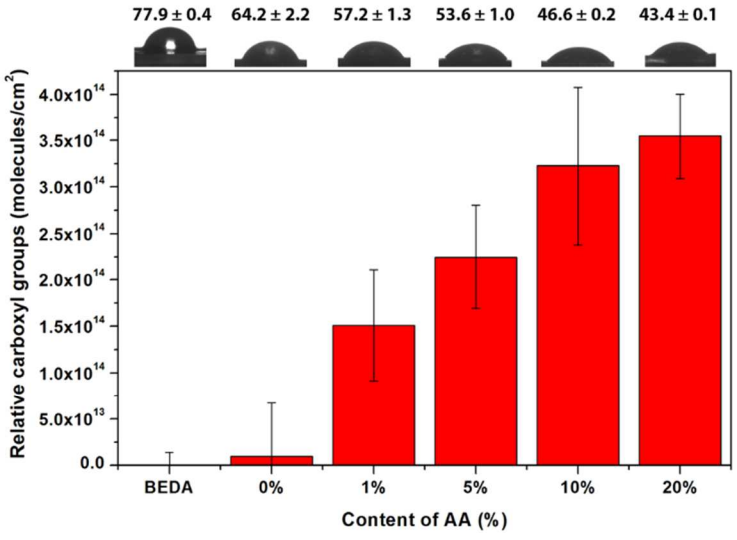

Figure 2. Relative quantification of the relative carboxyl groups with TBO, and water contact angle of BEDA samples (top).

As reported in Figure 2, the higher is the amount of AA in the polymer formulation, the higher is the final number of available carboxyl groups. In particular, the highest density of –COOH groups was reached with 10 and 20 % of AA, with a relative value of about $3.23 \pm 0.85 \times 10^{14}$ and $3.56 \pm 0.46 \times 10^{14}$ molecules/cm^2, respectively. At the same time, the presence of Reactive Orange (RO) dye was uninfluential on this kind of titration (0% sample), even if this Azo dye can be positively charged in basic conditions. Finally, this test confirmed the increased number of carboxyl groups into the polymer matrix, highlighting the possibility to tune the properties of the 3D printed device for the final biosensing application.

Once the material was physico-chemically characterized, in order to compare the grafting ability related to different AA content, a functional evaluation of the binding capability of the BEDA samples has been performed. The samples were firstly treated with EDC/sulfo-NHS to activate the carboxyl groups, then incubated in a solution of protein G (PtG) and finally with a goat anti-mouse IgG horseradish peroxidase conjugated (Ab-HRP). APTES/SA functionalized silicon samples, with the same dimension of BEDA+AA ones, were also included as reference for the well-known biomolecules binding ability of this procedure.[9, 45]

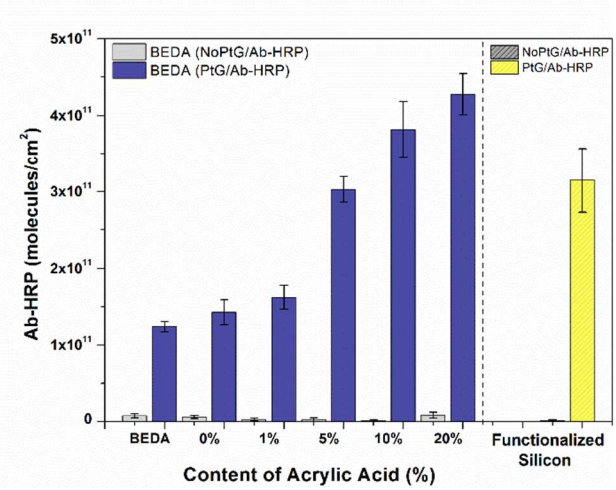

Figure 3. Comparison of the binding capability of BEDA and functionalized silicon samples by PtG/Ab-HRP bioassay

As shown in **Figure 3**, there is a strong correlation between the amount of AA in the polymer formulation and the Ab-HRP molecules density that is directly related to the PtG grafting ability of the different samples. Increasing the percentage of AA above 5% enhances the binding capability, obtaining a density of Ab-HRP molecules higher than the one obtained through silicon samples functionalized with the optimized and well-established APTES/SA protocol. Moreover, the increase of the binding capability is also combined to a faster sample fabrication procedure that does not require further functionalization steps, which is necessary for the silicon samples.

The amount of biomolecules bound to the bare BEDA polymer is probably due to physical absorption to the polymeric material, but could also be related to the formation of a secondary or tertiary amine-acrylate adduct, by Michael addition.[46] Instead, the presence of the RO dye did not significantly influence the biomolecules binding, in agreement with the quantification of the

–COOH functionalities. This functional bioassay demonstrates that the introduction of AA in the BEDA network enhances the ability to immobilize biomolecules, achieving even better results than those obtained with APTES/SA functionalized silicon samples.

3D Printing and analysis of microcantilevers

The MC structures were 3D printed according to the prepared CAD files reported in **Figure 4A**. In order to obtain a self-standing cantilever, after several experimental tests, the slicing thickness was set on the machine at 25 µm. The MCs were printed with a final device thickness of around 200 µm to strongly reduce bending of the cantilever tip. Then the length of the MCs was defined to obtain a geometry as close as possible to an ideal plate to gain the best mechanical performances. The final dimensions of the 3D printed MC were 3000 µm x 700 µm x 200 µm (length x width x thickness, see Figure 4B). In order to match binding capability and mechanical stiffness, the formulation containing 10% of AA was chosen for 3D printing of the MCs structures. These samples were subsequently characterized and used in the biological assay test. Even though the samples based on the formulation with 20% AA showed the higher binding capabilities, they suffered from a consistent worsening of the mechanical properties (lower elastic modulus, see Figure 1B) and thus the use of this formulation was not recommended.

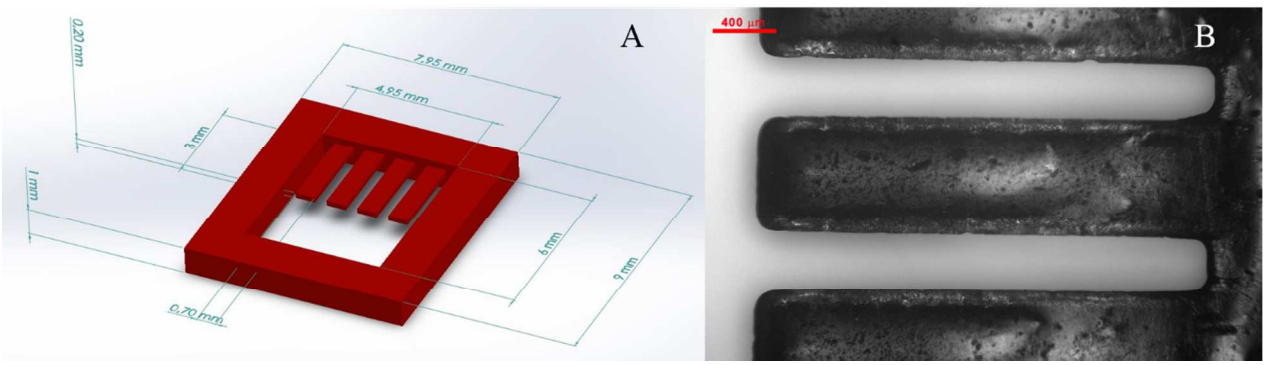

Figure 4. A) CAD design of the 3D printed MCs B) Optical image of the 3D printed MCs.

The mechanical properties of the printed MC were analyzed by means of Laser Doppler Vibrometer (LDV), which allows highly precise measurement of the vibration amplitude with sub-picometer resolution. The sensor arrays were actuated through a piezoelectric disk excited with sinusoidal waveforms at different frequencies and the values of the resonance frequencies were extracted from the vibration amplitude signal. The peaks related to the first and the second resonance modes are observable in the vibration spectra (**Figure 5)** with amplitude signal clearly above the background noise. Measuring the vibration spectrum in different point of the printed MC, the LDV is able to reconstruct a 3-D visualization of the device motion for each frequency (inset of Figure 4). As expected at the first resonance mode frequency of 27.910 kHz the polymeric cantilever is bending upward and downward with maximum deflection at the tip. Instead, at 156.748 kHz, the second resonance mode frequency, the microcantilever vibration shape presents fixed points at two-thirds of its length. Analyzing the cantilevers' resonant modes, it is possible to evaluate the elastic properties of the printed objects. In the case of a homogeneous, single material beam with a fixed end and a free one, the resonance frequencies are expressed as:

$$f_{r,n} = \frac{(k_n)^2}{2\pi}\frac{h}{l^2}\sqrt{\frac{E}{12\rho}} \quad (1)$$

where, h and l represent the thickness and length of the microcantilever, E the effective elastic modulus, ρ the material density and k_n is a constant value obtained from the boundary condition of the beam representing the mode of vibration.

Therefore, the effective elastic modulus can be computed as:

$$E = 12\rho\left(f_r \frac{2\pi}{(k_n)^2}\frac{l^2}{h}\right)^2 \quad (2)$$

Normally, for a crystalline or polycrystalline material, like silicon, the elastic modulus can be assumed independent from the excitation frequency. Instead, in polymeric materials, like BEDA, elastic modulus increases according with the frequency of the applied stress. In this case, the elastic modulus computed from the resonance mode analysis is around 0.9 GPa which is higher than the value obtained at room temperature with DMTA measurement (0.5 GPa measured at 1 Hz).

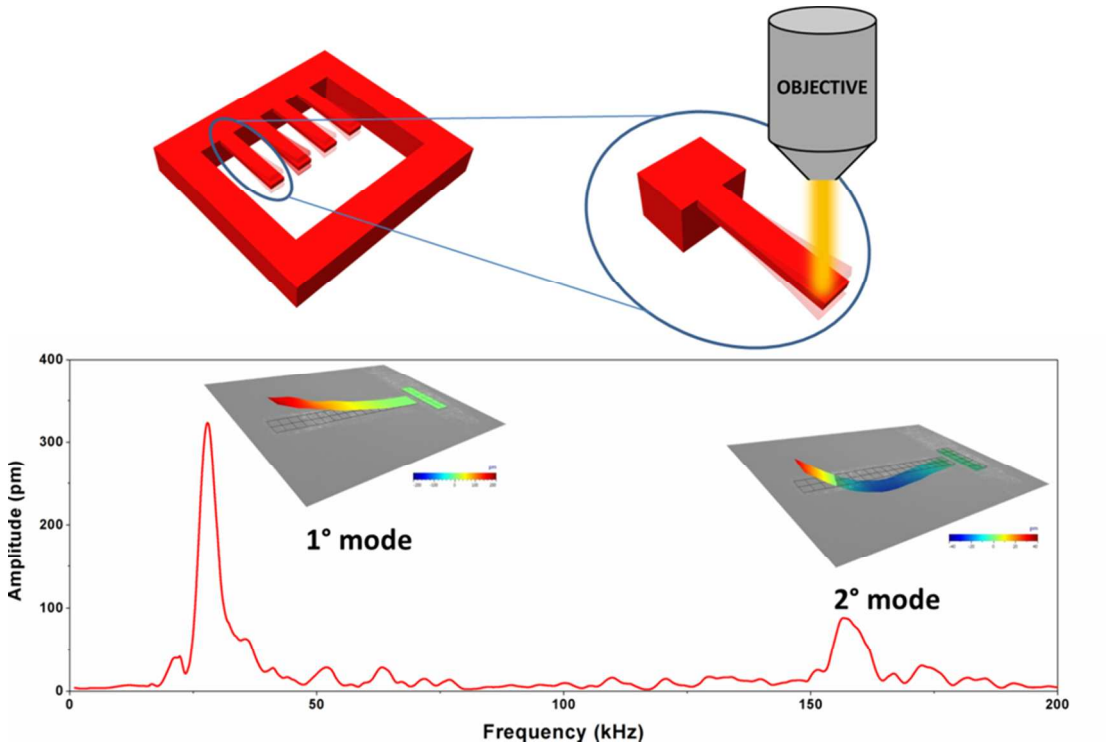

Figure 5. (Top) Schematic illustration of the 3D printed MCs arrays and their vibrational characterization by means of a LDV. (Bottom) Tip amplitude vibration spectrum of a polymeric cantilever. In the inset the 3-D visualization of the device experimental vibration amplitude at the first ($f_{r,1}$=27.910 kHz) and second ($f_{r,2}$=156.748 kHz) resonance frequency are represented.

In order to demonstrate their application as biosensors, the arrays of 3D printed microcantilevers were tested in a proof-of-concept immunoassay protocol. Four different arrays, of four cantilevers each, were evaluated: two arrays were used as negative controls, avoiding the PtG incubation step. The resonance frequencies of the microcantilevers were measured before and after the incubation with PtG and/or Ab-HRP. The mean relative frequency shift and its standard deviation were calculated from the average of the signal of the eight cantilevers treated with the same condition. For both PtG (**Figure 6A**) and Ab-HRP (Figure 5B) incubations, the cantilever mean relative frequency shift is conspicuously higher in comparison to the negative control

signal, due to the binding of the biomolecules to the surface. The 3D printed microcantilevers treated with PtG registered a 23 times higher signal if compared with the shift of the arrays incubated only in the buffer solution (negative controls). After the Ab-HRP incubation, the same cantilever arrays treated with PtG evidenced a mean relative frequency shift 26 times higher than the negative controls. This relative frequency variation is more than one order of magnitude higher in comparison to the signal obtain on flat and nanostructured silicon microcantilever arrays treated with the same bioassay protocol. [45] A validation of the results obtained by the microgravimetric analysis of the cantilever came from the colorimetric development performed on the MC arrays after their resonance frequencies characterization (Fig. 5D). The difference in the molecule surface density values obtained on positive and negative control samples is in good agreement with the results obtained from the analysis of the relative frequency shift. This demonstrates the feasibility of the proposed approach, introducing 3D printed polymer microcantilevers for biosensing applications.

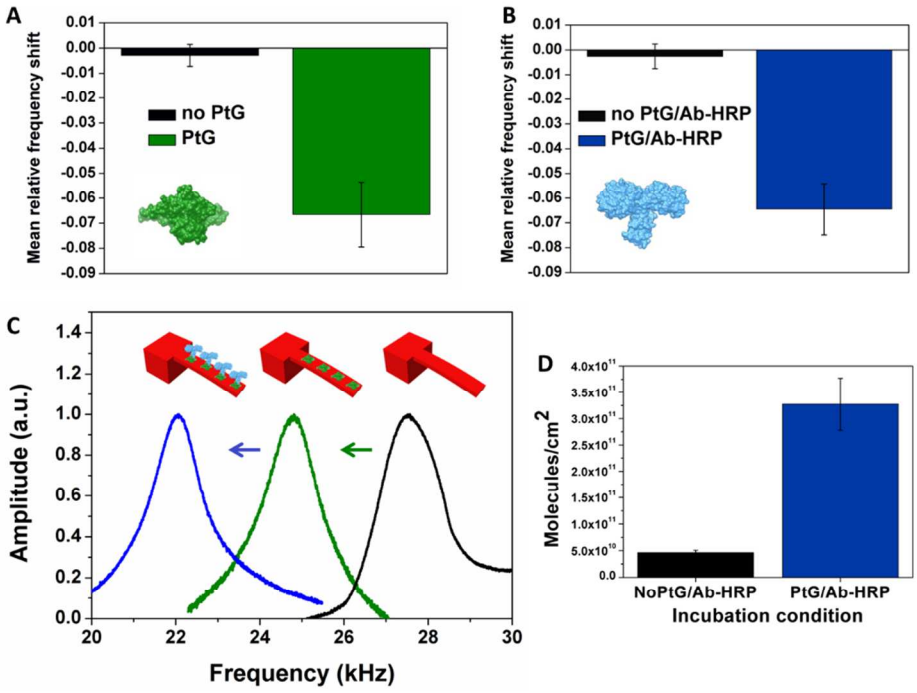

Figure 6 A) Comparison of the mean relative frequency shifts of 3D printed microcantilevers after PtG incubation. B) Comparison of the mean relative frequency shifts of 3D printed microcantilevers after Ab-HRP incubation. C) Variation of the resonance frequency before and after each bioassay step. D) Surface density of immobilized Ab-HRP on 3D printed microcantilevers obtained by colorimetric assay.

Conclusion

In this work, a novel approach for the fabrication of mass sensing biosensors is reported. Taking advantage of DLP-3D printing technology, we fabricated an array of microcantilevers in a single printing step, avoiding the time-costing microfabrication procedures necessary for standard silicon microcantilevers. Moreover, we were able to control the amount of available active carboxylic groups on the cantilevers, by adding acrylic acid as comonomer in the printable formulation, obtaining structures suitable for an easy enzymatic functionalization without any

further step, which is the case for actual microcantilevers technology. At last, 3D printed microarrays were tested in a standard immunoassay protocol, demonstrating to be suitable for biosensing applications. The proposed strategy represents an important improvement in microcantilever biosensor field, showing that taking advantage of 3D printing technology and properly controlling the printable formulation it is possible to fabricate sensor structures with intrinsic functionalities in a single step, paving the way to the development of a new class of simple mass biosensors.

ASSOCIATED CONTENT

Supporting Information. Sketch of 3D printing procedure, photorheology experiments and ATR analysis and spectra of the printed structures are reported in Supporting Information File.

AUTHOR INFORMATION

Corresponding Author

* ignazio.roppolo@iit.it, alessandro.chiado@polito.it

Author Contributions

The manuscript was written through contributions of all authors. All authors have given approval to the final version of the manuscript. ‡These authors contributed equally.

REFERENCES

1. Arlett, J. L.; Myers, E. B.; Roukes, M. L., Comparative Advantages of Mechanical Biosensors.*Nat. Nanotechnol.* **2011,** *6*, 203-215.

2. Ferrante, I.; Ciprianetti, N.; Stassi, S.; Santoro, K.; Ferrero, S.; Scaltrito, L.; Ricciardi, C., High-Throughput Characterization of Microcantilever Resonator Arrays for Low-Concentration Detection of Small Molecules. *J. Microelectromech. Syst.* **2017,** *26*, 246-254.

3. Malvar, O.; Ruz, J. J.; Kosaka, P. M.; Domínguez, C. M.; Gil-Santos, E.; Calleja, M.; Tamayo, J., Mass and Stiffness Spectrometry of Nanoparticles and Whole Intact Bacteria by Multimode Nanomechanical Resonators. *Nat. Commun.* **2016,** *7*, 13452.

4. Ricciardi, C.; Castagna, R.; Ferrante, I.; Frascella, F.; Luigi Marasso, S.; Ricci, A.; Canavese, G.; Lorè, A.; Prelle, A.; Lodovica Gullino, M.; Spadaro, D., Development of a Microcantilever-based Immunosensing Method for Mycotoxin Detection. *Biosens. Bioelectron.* **2013,** *40*, 233-239.

5. Yang, Y. T.; Callegari, C.; Feng, X. L.; Ekinci, K. L.; Roukes, M. L., Zeptogram-scale Nanomechanical Mass Sensing. *Nano Lett.* **2006,** *6*, 583-586.

6. Chaste, J.; Eichler, A.; Moser, J.; Ceballos, G.; Rurali, R.; Bachtold, A., A Nanomechanical Mass Sensor with Yoctogram Resolution. *Nat. Nanotechnol.* **2012,** *7*, 301-304.

7. Venstra, W. J.; Capener, M. J.; Elliott, S. R., Nanomechanical Gas Sensing with Nonlinear Resonant Cantilevers. *Nanotechnology* **2014,** *25*, 425501.

8. Stassi, S.; Cauda, V.; Fiorilli, S.; Ricciardi, C., Surface Area Enhancement by Mesoporous Silica Deposition on Microcantilever Sensors for Small Molecule Detection. *J. Mater. Chem. C* **2015,** *3*, 12507-12513.

9. Palmara, G.; Chiadò, A.; Calmo, R.; Ricciardi, C., Succinic Anhydride Functionalized Microcantilevers for Protein Immobilization and Quantification. *Anal. Bioanal. Chem.* **2016,** *408*, 7917-7926.

10. Zhou, S.; Yuan, L.; Hua, X.; Xu, L.; Liu, S., Signal Amplification Strategies for DNA and Protein Detection Based on Polymeric Nanocomposites and Polymerization: A Review. *Anal. Chim. Acta* **2015,** *877*, 19-32.

11. Seena, V.; Fernandes, A.; Pant, P.; Mukherji, S.; Ramgopal Rao, V., Polymer Nanocomposite Nanomechanical Cantilever Sensors: Material Characterization, Device Development and Application in Explosive Vapour Detection. *Nanotechnology* **2011,** *22*, 295501.

12. Zhang, Y.; Kim, H. H.; Kwon, B. H.; Go, J. S., Polymeric Cantilever Sensors Functionalized with Multiamine Supramolecular Hydrogel. *Sens. Actuators, B* **2013,** *178*, 47-52.

13. Mouaziz, S.; Boero, G.; Popovic, R. S.; Brugger, J., Polymer-based Cantilevers with Integrated Electrodes. *J. Microelectromech. Syst.* **2006,** *15*, 890-895.

14. Johansson, A.; Blagoi, G.; Boisen, A., Polymeric Cantilever-based Biosensors with Integrated Readout. *Appl. Phys. Lett.* **2006,** *89*, 173505.

15. Choi, Y. S.; Gwak, M. J.; Lee, D. W., Polymeric cantilever integrated with PDMS/Graphene Composite Strain Sensor. *Rev. Sci. Instrum.* **2016,** *87*, 105004.

16. Kim, D. S.; Jeong, Y. J.; Lee, B. K.; Shanmugasundaram, A.; Lee, D. W., Piezoresistive Sensor-integrated PDMS Cantilever: A New Class of Device for Measuring the Drug-induced Changes in the Mechanical Activity of Cardiomyocytes. *Sens. Actuators, B* **2017,** *240*, 566-572.

17. Chae, I.; Khan, M. F.; Song, J.; Kang, T.; Lee, J.; Thundat, T., Standoff Mechanical Resonance Spectroscopy Based on Infrared-Sensitive Hydrogel Microcantilevers. *Anal. Chem.* **2016,** *88*, 9678-9684.

18. Lee, J. S.; Song, J.; Kim, S. O.; Kim, S.; Lee, W.; Jackman, J. A.; Kim, D.; Cho, N.-J.; Lee, J., Multifunctional Hydrogel Nano-probes for Atomic Force Microscopy. *Nat. Commun.* **2016,** *7*, 11566.

19. Vaezi, M.; Seitz, H.; Yang, S., A review on 3D Micro-additive Manufacturing Technologies. *Int. J. Adv. Manuf. Tech.* **2013,** *67*, 1721-1754.

20. Hofmann, M., 3D Printing Gets a Boost and Opportunities with Polymer Materials. *ACS Macro Lett.* **2014,** *3*, 382-386.

21. Lin, D.; Nian, Q.; Deng, B.; Jin, S.; Hu, Y.; Wang, W.; Cheng, G. J., Three-dimensional Printing of Complex Structures: Man Made or Toward Nature? *ACS Nano* **2014,** *8*, 9710-9715.

22. de Leon, A. C.; Chen, Q.; Palaganas, N. B.; Palaganas, J. O.; Manapat, J.; Advincula, R. C., High Performance Polymer Nanocomposites for Additive Manufacturing Applications. *React. Funct. Polym.* **2016,** *103*, 141-155.

23. Martin, J. J.; Fiore, B. E.; Erb, R. M., Designing Bioinspired Composite Reinforcement Architectures via 3D Magnetic Printing. *Nat. Commun.* **2015,** *6*, 8641.

24. Lin, D.; Jin, S.; Zhang, F.; Wang, C.; Wang, Y.; Zhou, C.; Cheng, G. J., 3D Stereolithography Printing of Graphene Oxide Reinforced Complex Architectures. *Nanotechnology* **2015,** *26*, 434003.

25. Kalsoom, U.; Nesterenko, P. N.; Paull, B., Recent Developments in 3D Printable Composite Materials. *RSC Adv.* **2016,** *6*, 60355-60371.

26. Chiappone, A.; Fantino, E.; Roppolo, I.; Lorusso, M.; Manfredi, D.; Fino, P.; Pirri, C. F.; Calignano, F., 3D Printed PEG-Based Hybrid Nanocomposites Obtained by Sol–Gel Technique. *ACS Appl. Mater. Interfaces* **2016,** *8*, 5627-5633.

27. Fantino, E.; Chiappone, A.; Roppolo, I.; Manfredi, D.; Bongiovanni, R.; Pirri, C. F.; Calignano, F., 3D Printing of Conductive Complex Structures with in Situ Generation of Silver Nanoparticles. *Adv. Mater.* **2016,** *28*, 3712-3717.

28. Fantino, E.; Chiappone, A.; Calignano, F.; Fontana, M.; Pirri, F.; Roppolo, I., In Situ Thermal Generation of Silver Nanoparticles in 3D Printed Polymeric Structures. *Materials* **2016,** *9*, 589.

29. Peterson, G. I.; Schwartz, J. J.; Zhang, D.; Weiss, B. M.; Ganter, M. A.; Storti, D. W.; Boydston, A. J., Production of Materials with Spatially-Controlled Cross-Link Density via Vat Photopolymerization. *ACS Appl. Mater. Interfaces* **2016,** *8*, 29037-29043.

30. Cooperstein, I.; Layani, M.; Magdassi, S., 3D Printing of Porous Structures by UV-curable O/W Emulsion for Fabrication of Conductive Objects. *J. Mater. Chem. C* **2015,** *3*, 2040-2044.

31. Zhu, W.; Ma, X.; Gou, M.; Mei, D.; Zhang, K.; Chen, S., 3D Printing of Functional Biomaterials for Tissue Engineering. *Curr. Opin. Biotechnol.* **2016,** *40*, 103-112.

32. Palaganas, J.; de Leon, A. C.; Mangadlao, J.; Palaganas, N.; Mael, A.; Lee, Y. J.; Lai, H. Y.; Advincula, R., Facile Preparation of Photocurable Siloxane Composite for 3D Printing. *Macromol. Mater. Eng.* **2017**,DOI: 10.1002/mame.201600477.

33. Watanabe, T.; Akiyama, M.; Totani, K.; Kuebler, S. M.; Stellacci, F.; Wenseleers, W.; Braun, K.; Marder, S. R.; Perry, J. W., Photoresponsive Hydrogel Microstructure Fabricated by Two-Photon Initiated Polymerization. *Adv. Funct. Mater.* **2002,** *12*, 611-614.

34. Gomez, L. P. C.; Spangenberg, A.; Ton, X. A.; Fuchs, Y.; Bokeloh, F.; Malval, J. P.; Tse Sum Bui, B.; Thuau, D.; Ayela, C.; Haupt, K.; Soppera, O., Rapid Prototyping of Chemical Microsensors Based on Molecularly Imprinted Polymers Synthesized by Two-Photon Stereolithography. *Adv. Mater.* **2016**, *28*, 5931-5937.

35. Credi, C.; Fiorese, A.; Tironi, M.; Bernasconi, R.; Magagnin, L.; Levi, M.; Turri, S., 3D Printing of Cantilever-Type Microstructures by Stereolithography of Ferromagnetic Photopolymers. *ACS Appl. Mater. Interfaces* **2016,** *8*, 26332-26342.

36. Jackson, J. M.; Witek, M. A.; Hupert, M. L.; Brady, C.; Pullagurla, S.; Kamande, J.; Aufforth, R. D.; Tignanelli, C. J.; Torphy, R. J.; Yeh, J. J.; Soper, S. A., UV Activation of Polymeric High Aspect Ratio Microstructures: Ramifications in Antibody Surface Loading for Circulating Tumor Cell Selection. *Lab Chip* **2014,** *14*, 106-117.

37. Tiraferri, A.; Elimelech, M., Direct Quantification of Negatively Charged Functional Groups on Membrane Surfaces. *J. Membr. Sci.* **2012,** *389*, 499-508.

38. B Bhagwat, N.; Kiick, K. L.; Martin, D. C., Electrochemical Deposition and Characterization of Carboxylic Acid Functionalized PEDOT Copolymers. *J. Mater. Res.* **2014,** *29*, 2835-2844.

39. Chiadò, A.; Palmara, G.; Ricciardi, S.; Frascella, F.; Castellino, M.; Tortello, M.; Ricciardi, C.; Rivolo, P., Optimization and Characterization of a Homogeneous Carboxylic Surface Functionalization for Silicon-based Biosensing. *Colloids Surf., B* **2016,** *143*, 252-259.

40. Roppolo, I.; Messori, M.; Perruchas, S.; Gacoin, T.; Boilot, J. P.; Sangermano, M., Multifunctional Luminescent Organic/Inorganic Hybrid Films. *Macromol. Mater. Eng.* **2012,** *297*, 680-688.

41. Chiappone, A.; Jeremias, S.; Bongiovanni, R.; Schönhoff, M., NMR Study of Photo-Crosslinked Solid Polymer Electrolytes: The Influence of Monofunctional Oligoethers. *J. Polym. Sci., Part B: Polym. Phys.* **2013,** *51*, 1571-1580.

42. Hossain, M. D.; Lu, D.; Jia, Z.; Monteiro, M. J., Glass Transition Temperature of Cyclic Stars. *ACS Macro Lett.* **2014,** *3*, 1254-1257.

43. Podgórski, M.; Matynia, T., Network Structure/Mechanical Property Relationship in Multimethacrylates-Derivatives of Nadic Anhydride. *J. Appl. Polym. Sci.* **2008,** *109*, 2624-2635.

44. Schmidt, S.; Wang, H.; Pussak, D.; Mosca, S.; Hartmann, L., Probing Multivalency in Ligand-Receptor-Mediated Adhesion of Soft, Biomimetic Interfaces. *Beilstein J. Org. Chem.* **2015,** *11*, 720-729.

45. Stassi, S.; Chiadò, A.; Cauda, V.; Palmara, G.; Canavese, G.; Laurenti, M.; Ricciardi, C., Functionalized ZnO Nanowires for Microcantilever Biosensors with Enhanced Binding Capability. *Anal. Bioanal. Chem.* **2017,** *409*, 2615-2625.

46. Mather, B. D.; Viswanathan, K.; Miller, K. M.; Long, T. E., Michael Addition Reactions in Macromolecular Design for Emerging Technologies. *Prog. Polym. Sci.* **2006,** *31*, 487-531.

Table of Contents